Flat Clathrin Lattices Nucleate Reticular Adhesions in an Integrin β1 Activity-Dependent Manner

Laura Hakanpää[1,2], Amr Abouelezz[1,2], An-Sofie Lenaerts[1,2], Michael Algie[1,2], Jenny Bärlund[1,2], Pekka Katajisto[1,2,3,4], Harvey T. McMahon[5], Leonardo Almeida-Souza[1,2,4,*]

[1] Helsinki Institute of Life Science, HiLIFE, University of Helsinki, Helsinki, Finland.
[2] Institute of Biotechnology, University of Helsinki, Helsinki, Finland.
[3] Department of Cell and Molecular Biology, Karolinska Institutet, Stockholm, Sweden.
[4] Faculty of Biological and Environmental Sciences, University of Helsinki, Helsinki, Finland.
[5] MRC Laboratory of Molecular Biology, Cambridge, UK.

* Correspondence: leonardo.almeida-souza@helsinki.fi

Abstract

The molecular machinery involved in clathrin mediated endocytosis (CME) forms two distinct structures at the plasma membrane: clathrin coated pits and flat clathrin lattices. Clathrin coated pits are the canonical endocytic carriers for CME and have been extensively studied. In contrast, the cellular role of flat clathrin lattices, characterised by their stability, are not well understood. Here we show that flat clathrin lattices mediate the formation of a special type of cellular adhesions, called reticular adhesions, in a process controlled by the composition of the extracellular matrix. We observed that cells plated on fibronectin displayed few flat clathrin lattices and reticular adhesions. Notably, this effect occurred locally in cells, in an extracellular matrix-contact dependent manner. Inhibition of the CME machinery led to complete disappearance of reticular adhesions and live-cell imaging showed that flat clathrin lattice assembly is required for the establishment of reticular adhesions. Manipulation of the fibronectin receptor integrin β1 revealed that the formation of flat clathrin lattices - and consequently reticular adhesions - are controlled by the activity of this receptor. CME and other endocytic routes have conventionally been linked to the disassembly of cellular adhesions by mediating the internalisation of their components. Our results present a novel paradigm in the relationship between these two processes by showing that endocytic proteins can also play a role in the assembly of cellular adhesions.

Introduction

Clathrin-Mediated Endocytosis (CME) is the predominant route by which cells internalise nutrients, pathogens and membrane components (Kaksonen and Roux, 2018). The distinguishing feature of CME is the formation of short-lived and dynamic membrane invaginations covered by polygonal clathrin cages termed clathrin coated pits (CCPs) (Kaksonen and Roux, 2018; McMahon and Boucrot, 2011). The CME machinery also assembles into large, long-lived structures known as "clathrin plaques" or flat clathrin lattices (FCLs) (Grove et al., 2014). Despite having a similar molecular composition to CCPs, our understanding of the biology of FCLs is very limited. FCLs are considered as stalled endocytic events and recent studies support the idea that FCLs are signalling platforms (Alfonzo-Méndez et al., 2022; Grove et al., 2014; Leyton-Puig et al., 2017). *In vivo*, FCLs localise to adhesive structures between bone and osteoclasts (Akisaka et al., 2008) and are required for the organization of sarcomeres (Vassilopoulos et al., 2014). Notably, the cellular conditions and the cascade of events regulating the formation, maintenance and disassembly of FCLs are completely unknown.

Recent studies showed that FCLs localised to reticular adhesions (RAs), a long-lived and distinct cellular adhesion composed of integrin **α**v**β**5 and devoid of typical focal adhesion (FA) components (Lock et al., 2018; Zuidema et al., 2018). The cellular significance of this colocalisation remains largely unexplored.

Here, we show that the formation of RAs depends on FCLs. Moreover, we found that the composition of the extracellular matrix (ECM) is a master regulator of this process where fibronectin-activated integrin **β**1 acts as an inhibitor of the co-assembly of FCLs and RAs.

Results

ECM composition determines the ratio between CCPs and FCLs

While studying CME dynamics, we serendipitously observed that cells on fibronectin (FN) appears to display fewer FCLs. To confirm this finding, we measured the frequency of FCLs in U2OS cells with an endogenously GFP-tagged alpha adaptin 2 sigma subunit (AP2S1, hereafter referred to simply as AP2) plated on glass and FN (Fig. 1a,b). AP2 is a widely used CME marker (Almeida-Souza et al., 2018; Ehrlich et al., 2004; Rappoport and Simon, 2008). We opted to use an endogenously tagged cell line throughout this study as the expression level of this complex was reported to modulate FCL frequencies (Dambournet et al., 2018). Cells plated on glass presented many typical FCLs (i.e. bright, long-lived AP2-GFP marked endocytic structures) while cells on FN displayed predominantly typical CCPs (Fig. 1a-b). To further explore this observation, we compared FCL frequencies in cells plated on dishes coated with major ECM proteins FN, vitronectin (VTN), collagen I (Col I) and collagen IV (Col IV). As controls, we also plated cells on two non-ECM coatings, bovine serum albumin (BSA) and poly-L-lysine (PLL), or glass. This comparative analysis revealed that FN stands out from other matrix proteins and reduces FCL frequency most prominently (Fig. 1c, Fig. S1a, Supplementary video 1). Col IV and VTN reduced FCL frequency to some extent compared to glass and the non-ECM coatings (Fig. 1a, Fig. S1a, Supplementary video 1). The non-ECM proteins (BSA and PLL) had no FCL reducing effect. Interestingly, and in line with a recent study (Baschieri et al., 2018), Col I did not reduce FCLs (Fig. 1b, Fig. S1a, Supplementary video 1).

For many cell lines, it is common to find considerable variability in the presence of FCLs in culture. We thus decided to probe if this variability is due to differential FN production within the culture. Confirming this hypothesis, and providing an explanation for the variability of FCL profiles within cultures, we found that cells plated on glass that presented fewer FCLs were predominantly lying on top of an FN-rich region of the culture (Fig. S1b).

Next, we asked if the lowered FCL frequency observed in FN-coated samples is a cell-wide effect or specific to cellular regions in direct contact with the extracellular substrate. For that, we used patterned dishes containing FN-coated regions interspersed with uncoated (glass) regions, where single U2OS-AP2-GFP cells could

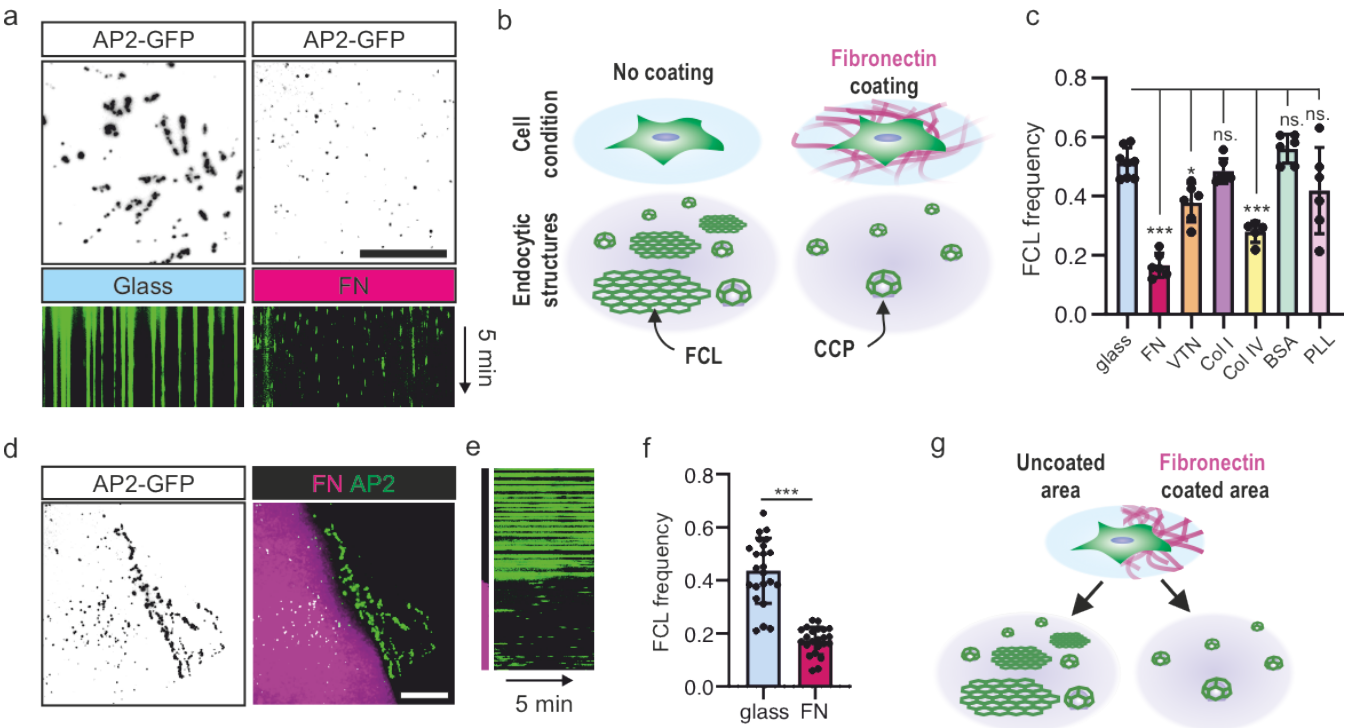

Figure 1. Fibronectin inhibits FCL formation in a local manner. ***a,*** *U2OS-AP2-GFP cells plated on glass or FN coated dishes were imaged using TIRF microscopy, 1 s intervals for 5 min. Representative time projections (15 s) and kymographs (5 min) of time-lapse videos.* ***b,*** *schematic illustration of results in (a).* ***c,*** *FCL frequency of U2OS-AP2-GFP cells plated on glass, FN, VTN, Col I, Col IV, BSA or PLL coated dishes and imaged using TIRF microscopy, 1 s intervals for 5 min. Glass: n=7 videos; FN, VTN, BSA, PLL: n=6 videos; Col I, Col IV: n=5 videos; One-way ANOVA with Tukey's multiple comparison test.* ***d-f,*** *U2OS-AP2-GFP cells plated on FN/glass patterned imaging dishes and imaged with TIRF microscopy using 1 s intervals for 5 min, representative time projections (15 s) (d) and kymographs (5 min) (e) of time-lapse video.* ***f,*** *Region-specific FCL frequency for (d,e), n=11 videos, two-tailed Student's t-test, P<0.001.* ***g***, *schematic illustration of results shown in d-f. Scale bars 10 µm. Data are the mean ± SD, ns. non-significant p-value;* * *p-value < 0.05;* *** *p-value < 0.001.*

adhere simultaneously to both FN and glass. In line with a contact-dependent effect, few FCLs were observed in cellular regions in contact with FN whereas FCLs were abundant in the cellular regions contacting glass (Fig. 1d-g, Supplementary video 2).

The abundance of an alternative splice variant of the clathrin heavy chain containing exon 31 was recently shown to increase the frequency of FCLs (Moulay et al., 2020). We thus decided to test if the effects we observe are due to changes in clathrin splicing but found no difference when comparing cells plated on uncoated or FN-coated dishes (Fig. S1c).

Thus, the formation of FCLs is controlled by the composition of the extracellular matrix with FN being a strong inhibitor of FCL formation. Importantly, this control occurs in a local manner, where FCL inhibition depends on direct contact with the ECM (Fig. 1g).

Fibronectin locally inhibits Reticular Adhesions

Reticular adhesions (RAs) are composed of integrin **αvβ**5 and are the only type of cellular adhesion maintained during mitosis, playing important roles controlling this process and ensuring spatial memory between cell generations (Lock et al., 2018). FCLs were shown to localise to RAs (Zuidema et al., 2018). However, the significance of this colocalisation is largely unexplored.

First, we confirmed these previous finding in our model system. Indeed, U2OS-AP2-GFP cells plated on glass and stained for integrin **αvβ**5 and the FA markers phosphorylated paxillin (p-PAX Y118) or phosphorylated Focal Adhesion Kinase (p-FAK Y397) displayed RAs which were positive for bright AP2-GFP puncta (i.e. FCLs) but not the FA markers, as reported (Lock et al., 2018; Wehrle-Haller, 2012; Zuidema et al., 2018) (Fig. 2a,b; Fig. S2a,b). Furthermore, RAs could also be differentiated from FAs for the absence of associated actin stress fibres (Fig. S2c).

Next, given the strong effects of FN on FCLs, we asked how FN coating affected RAs. Strikingly, cells plated on patterned FN revealed that RAs, akin to FCLs, were completely inhibited on cellular regions in contact with FN. The glass side of coverslips displayed many FCLs colocalising to RAs while on the FN-coated side, neither RAs nor FCLs were present (Fig. 2c-e). While in patterned substrates most of the integrin **αvβ**5 signal segregated to glass regions forming typical RAs (Fig. 2c,d), the integrin **αvβ**5 signal localised to FAs in cells plated on fully coated FN dishes (Fig. S3). Interestingly, the amount of integrin **αvβ**5 signal localising to FAs decreased with cell density (Fig. S3).

In line with previous observations (Baschieri et al., 2018; Zuidema et al., 2018), FCL formation was dependent on integrin **αvβ**5 as U2OS AP2-GFP cells silenced for integrin **β**5 displayed a lower FCL frequency compared to control cells (Fig. S4a-c). Integrin

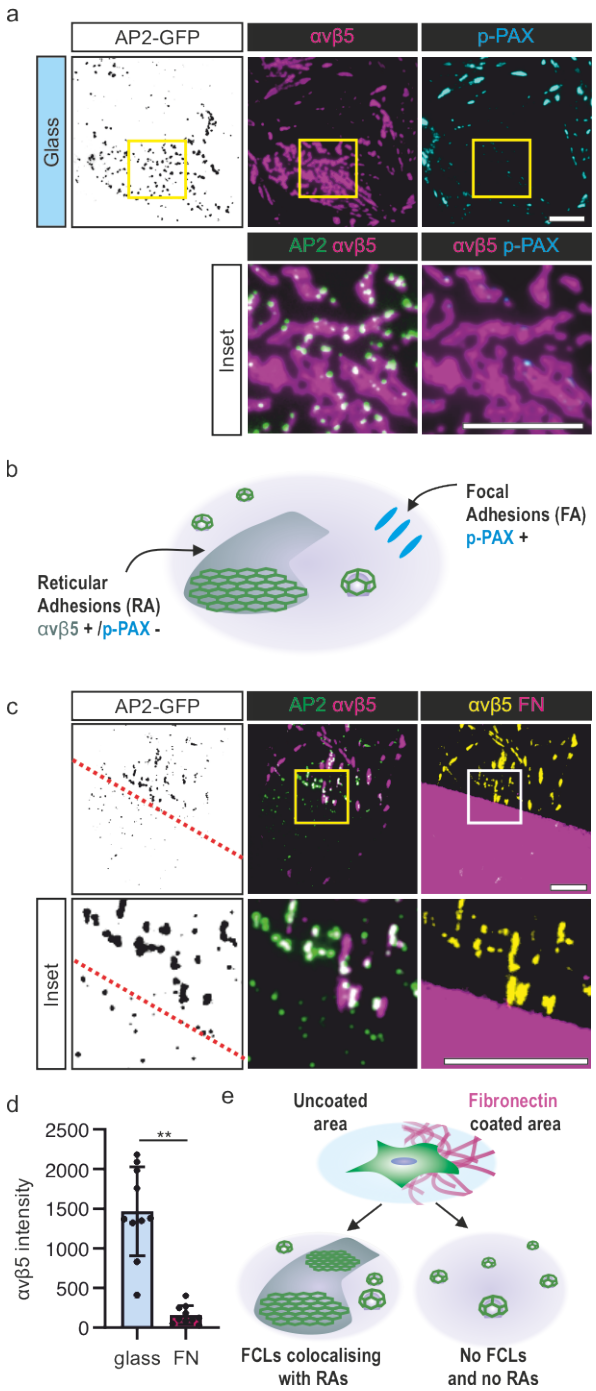

Figure 2. Fibronectin inhibits RA formation in a local manner. a, *U2OS-AP2-GFP cells plated on glass were stained for integrin αvβ5 and phopho-paxillin Y118 (p-PAX) and imaged using TIRF microscopy.* ***b,*** *schematic illustration of the results shown in (a).* ***c,d,*** *U2OS-AP2-GFP cells were plated on FN/glass patterned imaging dishes overnight, stained for integrin αvβ5 and p-PAX, and imaged using TIRF microscopy, representative TIRF images (c) and quantification of integrin αvβ5 intensity on FN- and glass-side of the pattern (d), n=10, two-tailed Student's t-test.* ***e,*** *schematic illustration of results shown in (c,d). Scale bars 10 μm. Data are the mean ± SD, ** p-value < 0.01.*

β5 silenced cells were unable to form RAs, but formed FAs (Fig. S4a,d). The dependency of integrin β5 on FCL formation was further confirmed using Cilengitide, the inhibitor for integrin αvβ5 (Desgrosellier and Cheresh, 2010), as the treatment led to a rapid disassembly of FCLs (Fig. S5).

Hence, the composition of the extracellular matrix controls the formation of RAs and FCLs in a very similar manner (Fig. 2e), suggesting a common mechanism for the establishment of these structures.

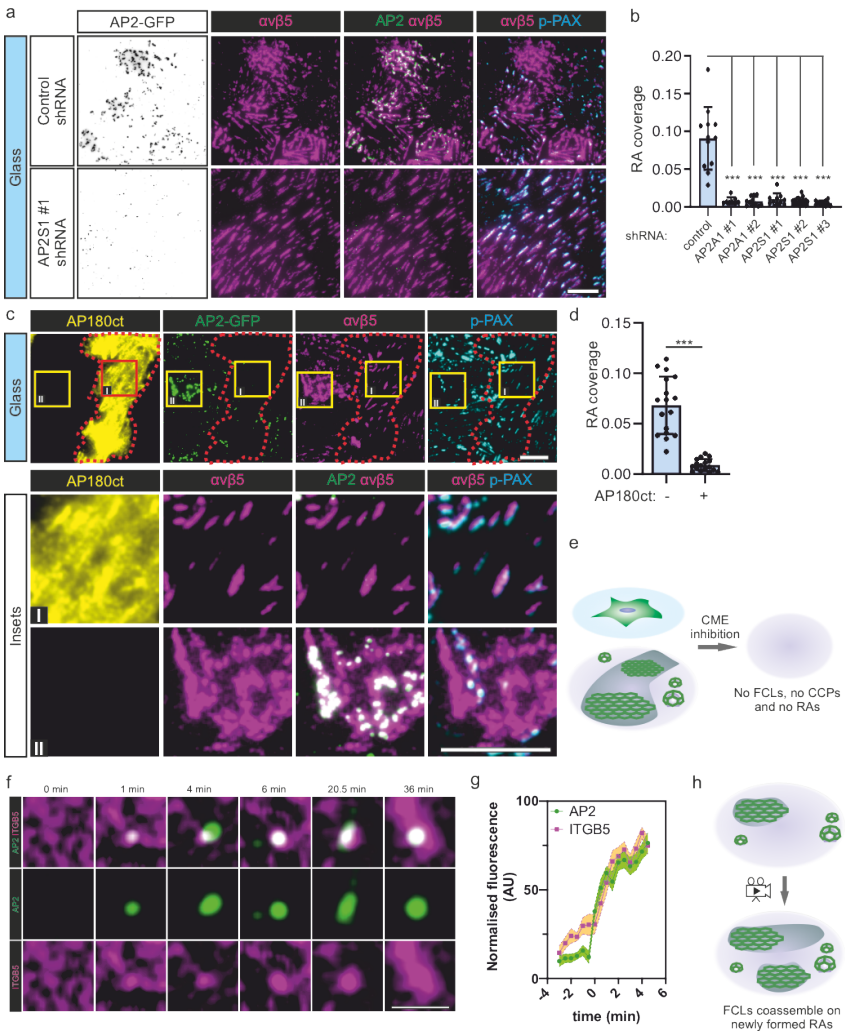

Figure 3. Inhibition of CME prevents FCL and RA formation. a,b, *U2OS-AP2-GFP cells silenced for AP2 subunits alpha 1 (AP2A1) or sigma 1 (AP2S1) with five shRNAs or control (scrambled shRNA) were plated on glass, stained for integrin αvβ5 and p-PAX and imaged using TIRF microscopy.* ***a,*** *representative TIRF images of control and AP2S1 subunit (shAP2S1 #1) silenced cells. Representative pictures for all shRNAs used are shown in Figs S7, S8.* ***b,*** *analysis of RA coverage of AP2 silenced cells, control n=12, shAP2A1#1 n=8, shAPA1#2 n=11, shAPS1#1, #3 n=10, shAPS1#2 n=19, One-way ANOVA with Tukey's multiple comparison.* ***c,d,*** *U2OS-AP2-GFP cells overexpressing Ap180ct were plated on glass and stained for integrin αvβ5 and p-PAX, imaged with TIRF microscopy, representative TIRF images (c) and analysis of RA coverage (d), n=17, two-tailed Student's t-test.* ***e,*** *Schematic illustration of results shown in a-d.* ***f,g,*** *U2OS-AP2-GFP-ITGB5-mScarlet cells plated on glass were treated with Cilengitide (10 μM) for 15 min, washed, and imaged using TIRF microscopy at 2 frames per minute, a representative event (f and Supplementary video 3) and analysis of AP2 and ITGB5 intensity over time (g) (n = 16 events).* ***h,*** *schematic illustration of results shown in (f,g). Scale bars 10 μm (a,c) and 2 μm (f). Data are the mean ± SD, *** p-value < 0.001 or mean ± SEM in (g).*

The CME machinery nucleates RA formation

While all FCLs colocalise to RAs, the opposite is not true (Fig. 2a, Fig. S2), which may give the impression that FCLs are formed on existing RAs. Nevertheless, the fact that both structures are inhibited independently by FN suggests a deeper relationship, and led us to ask if RAs can exist without the CME machinery. To answer this question, we quantified the amount of RAs in U2OS-AP2-GFP cells silenced for the clathrin adaptor AP2 complex subunits alpha 1 (AP2A1) or sigma 1 (AP2S1). Cells for this experiment were plated on glass to support RA formation. Consistent with a key role played by the CME machinery in RA formation, AP2A1 or AP2S1 silenced cells (easily recognisable as cells with little to no AP2-GFP signal), did not display RAs. Instead, integrin αvβ5 localised to the FA marker, while control cells displayed prominent RAs (Fig. 3a,b; Figs S6, S7).

To confirm these results, we expressed the AP180 C-terminal fragment (AP180ct), which acts as a strong dominant negative of CME (Ford et al., 2001). AP180ct-positive U2OS-AP2-GFP cells on glass displayed low AP2 signal at the membrane and, akin to AP2 silenced cells, RAs were largely absent with integrin αvβ5 localised to FAs, whereas AP180ct-negative cells displayed typical FCLs and RAs (Fig. 3c-e).

Next, we set out to visualise the dynamics of AP2 during RA formation. For that, we generated a double U2OS knock-in cell line - AP2-GFP and Integrin β5 (ITGB5)-mScarlet. RAs are remarkably stable structures (Lock et al., 2018) and their *de novo* formation is rare, making it difficult to capture such events. To overcome this problem, we optimised the conditions for Cilengitide treatment to disassemble RAs followed by a washout, when RAs could start reforming (Fig. S8). Using these washout conditions, we were able to capture

events which showed that the formation and growth of ITGB5-postive structures are accompanied by the formation of FCLs (Fig. 3f,g; Fig. S9; Supplementary videos 3,4). Also, in events where we could not clearly detect the extension of a mature RA, we noticed that the establishment of an FCL was typically accompanied by an increase in ITGB5 fluorescence (Fig. 3g; Fig. S9).

Taken together, our results show that the relationship between FCLs and RAs is beyond a simple colocalisation. In fact, our data reveals a strict co-dependency, where FCLs are required for the initial integrin **αv β5** clustering required for RA formation (Fig. 3e,h).

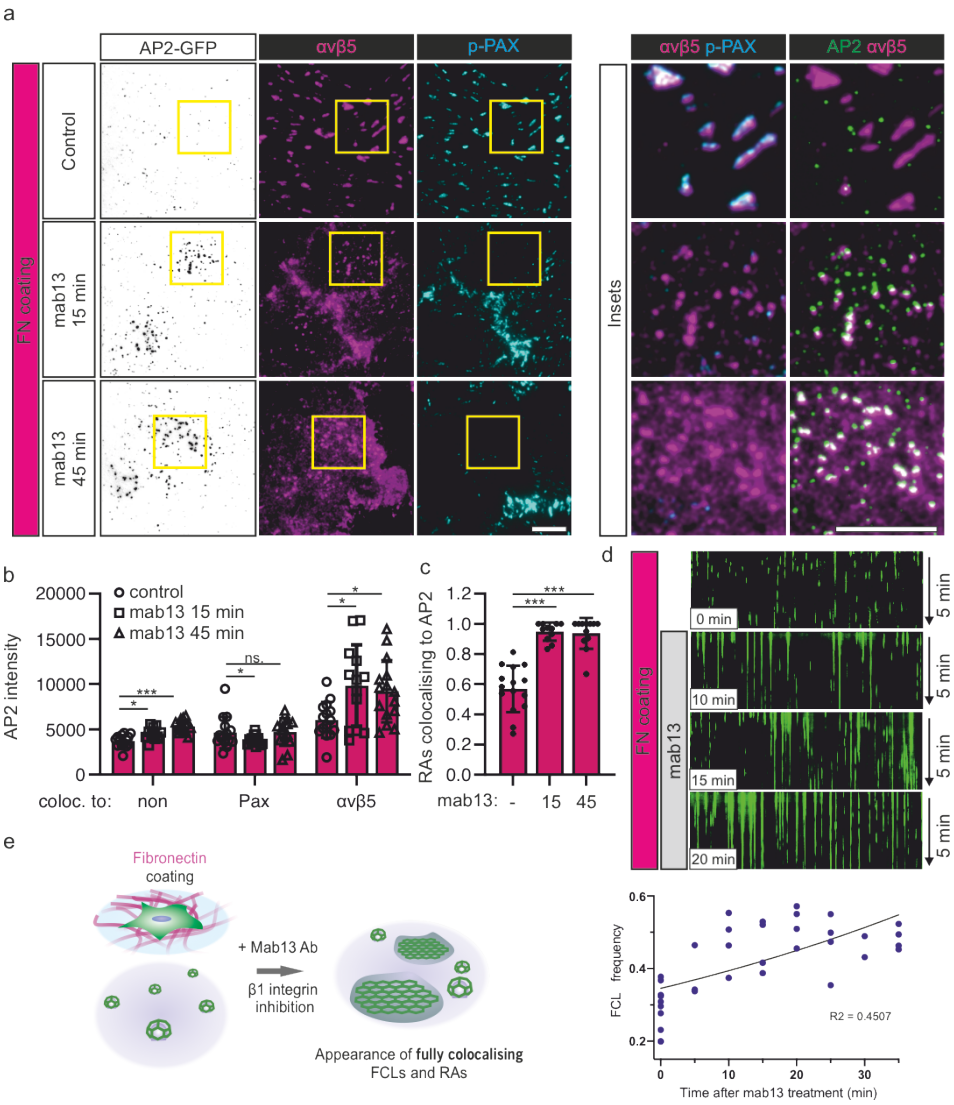

***Figure 4. Integrin β1 blocking stimulates FCL and RA formation**. **a-c,** U2OS-AP2-GFP cells plated on FN were treated with integrin β1 blocking antibody mab13 (0.3 μg/ml) for 15 and 45 min (or vehicle for 45 min = control), stained for integrin αvβ5 and p-PAX and imaged using TIRF microscopy, representative TIRF images (a) and analysis of AP2 signal (b): not colocalising with any markers (non) or localizing with p-PAX or integrin αvβ5 over time, n=18 for control, n=13 for mab13 15 min, n=15 for mab13 45 min, One-way ANOVA with Tukey's multiple comparison. **c,** analysis of fraction of integrin αvβ5 colocalising with AP2 over time, control n=15, mab13 15 min n=11, mab13 45 min n=12, One-way ANOVA with Tukey's multiple comparison. **d,** U2OS-AP2-GFP cells plated on FN were treated with mab13 (0.3 μg/ml) and imaged using TIRF microscopy, 1 s intervals for 5 min starting at 0 min (no mab13) and every 5 min after mab13 addition until 35 min, n=32 videos, One-way ANOVA with Tukey's multiple comparison, F(7, 29)=8.893, P<0.001. **e,** schematic illustration of results shown in (a-c). Scale bars 10 μm. Data are the mean ± SD,* p-value<0.05, *** p-value < 0.001.*

Matrix binding of integrin β1 controls RA and FCL formation

To understand the mechanism controlling the co-assembly of FCLs and RAs we turned our attention back to FN. We focused on integrin **β**1, which forms heterodimers that function as major FN receptors (Humphries et al., 2006). First, we acutely interfered with integrin **β**1's capacity to bind FN using the function-blocking antibody mab13. U2OS-AP2-GFP cells seeded on FN coated dishes were treated with mab13 and observed for the formation of FCLs and RAs. Over the time course of 45 min, mab13 induced the relocalisation of integrin **αv β**5 from FAs to small, newly formed RAs (Fig. 4a,b). Further supporting the role of FCLs in RA assembly, these newly formed RAs completely colocalised with FCLs (bright AP2 signals) (Fig. 4c). A similar experiment followed by live-cell imaging confirmed these results and showed an increase in FCL frequency after mab13 treatment (Fig. 4d). Mab13 treatment had no effect on existing FCLs and RAs formed on glass (Fig. S10). In concert with the results above, integrin **β**1 silenced U2OS-AP2-GFP cells plated on FN had a high FCL frequency and prominent RAs (Fig. 5, Fig. S11). Thus, the activation of integrin **β**1 by extracellular FN inhibits the formation of RAs and FCLs.

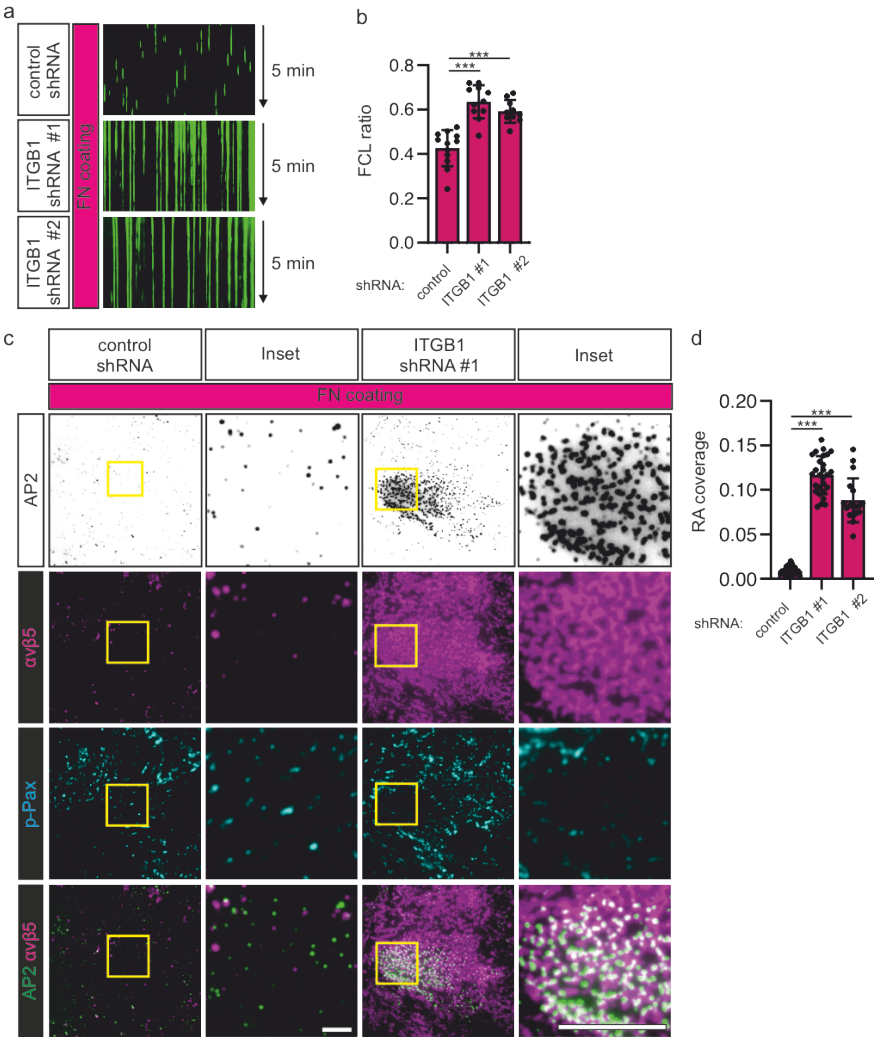

Figure 5. Depletion of integrin β1 promotes FCL and RA formation. a-d, *U2OS-AP2-GFP cells silenced for integrin β1 with two different shRNAs (shITGB#1, #2) or control shRNA were plated on FN and imaged using TIRF microscopy 1 s intervals for 5 min (a,b), or stained for integrin αvβ5 and p-PAX and imaged using TIRF microscopy (c,d).* ***a,b,*** *Representative kymographs of 5 min time-lapse videos (a), and analysis of FCL ratio from time-lapse videos (b), shScr n=12 videos, shITGB1 #1 n=11 videos, shITGB1 #2 n=10 videos, Tukey's multiple comparison.* ***c,d,*** *Representative TIRF images (c) and RA coverage analysis (d), control shRNA n=30, shITGB1 #1 n=27, shITGB1 #2 n=18, One-way ANOVA with Tukey's multiple comparison. Scale bars 10 μm. Data are the mean ± SD, *** p-value < 0.001.*

Discussion

The extracellular environment is a key regulator of cellular physiology with integrins playing a key role translating the chemical composition of the extracellular milieu into intracellular signals. Among various mechanisms controlling integrin function, integrin trafficking via endocytosis and exocytosis plays a major role (Moreno-Layseca et al., 2019). Thus far, the relationship between integrin-based matrix adhesions and endocytosis has been considered primarily antagonistic, with endocytosis playing a role in the disassembly of said adhesive structures (Ezratty et al., 2009; Moreno-Layseca et al., 2019). Here we provide evidence, for the first time, of a constructive relationship between the endocytic machinery and cellular adhesions. We present a novel mechanism where the CME machinery, in the form of FCLs, is key for the formation of integrin **αv**β5-based RAs.

We observed that FCL-mediated RA nucleation events are extremely rare, which led us to use a cilengitide washout experiment to detect them. For this reason, the trigger for the formation of FCLs and establishment of RAs remains to be understood. Recent evidence showed that EGFR activation led to the enlargement of FCLs in an integrin **β**5 phosphorylation-dependent manner (Alfonzo-Méndez et al., 2022), pointing to a possible mechanism for the initial co-assembly of FCLs and RAs. This possibility is further reinforced by the fact that the relationship between growth factor receptors and integrins has been established in multiple contexts (Ivaska and Heino, 2011).

Another key unknown aspect of FCL-mediated RA nucleation concerns how these structures can be molecularly differentiated from canonical endocytic events. The connection between integrin **αv**β5 located in RAs and FCLs occurs primarily via the endocytic adaptors ARH and NUMB (Zuidema et al., 2018). Importantly, these adaptors also participate in integrin endocytosis (Ezratty et al., 2009; Nishimura and Kaibuchi, 2007), suggesting that other mechanisms may be required to define the identity of FCLs.

Recently, a correlation was found between the presence of FCLs and an alternatively spliced isoform of clathrin containing exon 31 (Moulay et al., 2020). We did not detect any changes in clathrin splicing in our experimental system, which was not surprising given the effects we see are contact-dependent and could not be explained by transcriptional changes. Nonetheless, it is possible that the abundance of the exon 31-positive clathrin isoform works as a dial that changes the probability, speed or efficiency by which cells form FCLs.

We propose the following model for the formation of RAs by FCLs. In the absence (or low levels) of FN, the CME machinery binds to integrin **αv**β5 on the plasma membrane via adaptors

without triggering its internalisation. Polymerisation of clathrin establishes an FCL leading to integrin **α**v**β**5 clustering and formation of a nascent RA. These newly formed RAs can then further expand, outgrowing the FCL. In conditions of abundant FN, high levels of integrin **β**1 are activated leading to FCL inhibition and integrin **α**v**β**5 accumulation on FAs. The mechanism behind the RA-expansion beyond FCLs after their nucleation, or the molecular players linking integrin **β**1 activation to FCL inhibition are not known and are key questions for further investigation.

RAs persist during mitosis and their integrity is essential to maintain the division axis in cells, ensuring directional and efficient cytokinesis (Lock et al., 2018). Our results raise the intriguing possibility that the composition of the ECM, in combination with its orientation (Théry et al., 2005), can be used by cells to locally control RA formation – and, consequently, mitotic directionality – during development. The requirement of FN accumulation during branching morphogenesis of salivary glands (Sakai et al., 2003) supports this hypothesis.

In addition to its endocytic function, the clathrin machinery has been shown to participate in other processes. For example, clathrin helps to stabilise the mitotic spindle by binding to microtubules (Royle, 2012) and, during E. coli infection, the CME machinery is co-opted to form a clathrin-based actin-rich adhesive structure for the bacteria called pedestal (Veiga et al., 2007). Furthermore, a clathrin/AP2 tubular lattice was recently described to envelop collagen fibres during cell migration (Elkhatib et al., 2017). The results we present here add to this list of non-endocytic functions of CME components with an important twist. FCLs can also be disassembled into individual endocytic events (Lampe et al., 2016; Maupin and Pollard, 1983; Tagiltsev et al., 2021), providing an elegant and efficient mechanism for cells to switch the same machinery from an adhesion assembly to an adhesion disassembly function.

References

Akisaka, T., Yoshida, H., Suzuki, R., and Takama, K. (2008). Adhesion structures and their cytoskeleton-membrane interactions at podosomes of osteoclasts in culture. Cell Tissue Res. *331*, 625–641.

Alfonzo-Méndez, M.A., Sochacki, K.A., Strub, M.-P., and Taraska, J.W. (2022). Dual clathrin and integrin signaling systems regulate growth factor receptor activation. Nat. Commun. *13*, 905.

Almeida-Souza, L., Frank, R.A.W., García-Nafría, J., Colussi, A., Gunawardana, N., Johnson, C.M., Yu, M., Howard, G., Andrews, B., Vallis, Y., et al. (2018). A Flat BAR Protein Promotes Actin Polymerization at the Base of Clathrin-Coated Pits. Cell *174*, 325-337.e14.

Baschieri, F., Dayot, S., Elkhatib, N., Ly, N., Capmany, A., Schauer, K., Betz, T., Vignjevic, D.M., Poincloux, R., and Montagnac, G. (2018). Frustrated endocytosis controls contractility-independent mechanotransduction at clathrin-coated structures. Nat. Commun. 2018 91 *9*, 1–13.

Dambournet, D., Sochacki, K.A., Cheng, A.T., Akamatsu, M., Taraska, J.W., Hockemeyer, D., and Drubin, D.G. (2018). Genome-edited human stem cells expressing fluorescently labeled endocytic markers allow quantitative analysis of clathrin-mediated endocytosis during differentiation. J. Cell Biol. *217*, 3301–3311.

Desgrosellier, J.S., and Cheresh, D.A. (2010). Integrins in cancer: biological implications and therapeutic opportunities. Nat. Rev. Cancer *10*, 9–22.

Ehrlich, M., Boll, W., Van Oijen, A., Hariharan, R., Chandran, K., Nibert, M.L., and Kirchhausen, T. (2004). Endocytosis by Random Initiation and Stabilization of Clathrin-Coated Pits. Cell *118*, 591–605.

Elkhatib, N., Bresteau, E., Baschieri, F., Rioja, A.L., van Niel, G., Vassilopoulos, S., and Montagnac, G. (2017). Tubular clathrin/AP-2 lattices pinch collagen fibers to support 3D cell migration. Science *356*.

Ezratty, E.J., Bertaux, C., Marcantonio, E.E., and Gundersen, G.G. (2009). Clathrin mediates integrin endocytosis for focal adhesion disassembly in migrating cells. J. Cell Biol. *187*, 733–747.

Ford, M.G.J., Pearse, B.M.F., Higgins, M.K., Vallis, Y., Owen, D.J., Gibson, A., Hopkins, C.R., Evans, P.R., and McMahon, H.T. (2001). Simultaneous binding of PtdIns (4,5) P2 and clathrin by AP180 in the nucleation of clathrin lattices on membranes. Science (80-.). *291*, 1051–1055.

Grove, J., Metcalf, D.J., Knight, A.E., Wavre-Shapton, S.T., Sun, T., Protonotarios, E.D., Griffin, L.D., Lippincott-Schwartz, J., and Marsh, M. (2014). Flat clathrin lattices: Stable features of the plasma membrane. Mol. Biol. Cell *25*, 3581–3594.

Humphries, J.D., Byron, A., and Humphries, M.J. (2006). Integrin ligands at a glance. J. Cell Sci. *119*, 3901–3903.

Ivaska, J., and Heino, J. (2011). Cooperation Between Integrins and Growth Factor Receptors in Signaling and Endocytosis. Annu. Rev. Cell Dev. Biol. *27*, 291–320.

Jaqaman, K., Loerke, D., Mettlen, M., Kuwata, H., Grinstein, S., Schmid, S.L., and Danuser, G. (2008). Robust single-particle tracking in live-cell time-lapse sequences. Nat. Methods 2008 58 *5*, 695–702.

Kaksonen, M., and Roux, A. (2018). Mechanisms of clathrin-mediated endocytosis. Nat. Rev. Mol. Cell Biol. *19*, 313–326.

Lampe, M., Vassilopoulos, S., and Merrifield, C. (2016). Clathrin coated pits, plaques and adhesion. J. Struct. Biol. *196*, 48–56.

Leyton-Puig, D., Isogai, T., Argenzio, E., Van Den Broek, B., Klarenbeek, J., Janssen, H., Jalink, K., and Innocenti, M. (2017). Flat clathrin lattices are dynamic actin-controlled hubs for clathrin-mediated endocytosis and signalling of specific receptors. Nat. Commun. 2017 81 *8*, 1–14.

Lock, J.G., Jones, M.C., Askari, J.A., Gong, X., Oddone, A., Olofsson, H., Göransson, S., Lakadamyali, M., Humphries, M.J., and Strömblad, S. (2018). Reticular

adhesions are a distinct class of cell-matrix adhesions that mediate attachment during mitosis. Nat. Cell Biol. 2018 2011 *20*, 1290–1302.

Maupin, P., and Pollard, T.D. (1983). Improved preservation and staining of HeLa cell actin filaments, clathrin-coated membranes, and other cytoplasmic structures by tannic acid-glutaraldehyde-saponin fixation. J. Cell Biol. *96*, 51–62.

McMahon, H.T., and Boucrot, E. (2011). Molecular mechanism and physiological functions of clathrin-mediated endocytosis. Nat. Rev. Mol. Cell Biol. *12*, 517–533.

Moreno-Layseca, P., Icha, J., Hamidi, H., and Ivaska, J. (2019). Integrin trafficking in cells and tissues. Nat. Cell Biol. 2019 212 *21*, 122–132.

Moulay, G., Lainé, J., Lemaître, M., Nakamori, M., Nishino, I., Caillol, G., Mamchaoui, K., Julien, L., Dingli, F., Loew, D., et al. (2020). Alternative splicing of clathrin heavy chain contributes to the switch from coated pits to plaques. J. Cell Biol. *219*.

Nishimura, T., and Kaibuchi, K. (2007). Numb Controls Integrin Endocytosis for Directional Cell Migration with aPKC and PAR-3. Dev. Cell *13*, 15–28.

Rappoport, J.Z., and Simon, S.M. (2008). A Functional GFP Fusion for Imaging Clathrin-Mediated Endocytosis. Traffic *9*, 1250–1255.

Royle, S.J. (2012). The role of clathrin in mitotic spindle organisation. J. Cell Sci. *125*, 19–28.

Saffarian, S., Cocucci, E., and Kirchhausen, T. (2009). Distinct Dynamics of Endocytic Clathrin-Coated Pits and Coated Plaques. PLOS Biol. *7*, e1000191.

Sakai, T., Larsen, M., and Yamada, K.M. (2003). Fibronectin requirement in branching morphogenesis. Nat. 2003 4236942 *423*, 876–881.

Tagiltsev, G., Haselwandter, C.A., and Scheuring, S. (2021). Nanodissected elastically loaded clathrin lattices relax to increased curvature. Sci. Adv. *7*, 9934–9947.

Théry, M., Racine, V., Pépin, A., Piel, M., Chen, Y., Sibarita, J.B., and Bornens, M. (2005). The extracellular matrix guides the orientation of the cell division axis. Nat. Cell Biol. 2005 710 *7*, 947–953.

Vassilopoulos, S., Gentil, C., Lainé, J., Buclez, P.O., Franck, A., Ferry, A., Précigout, G., Roth, R., Heuser, J.E., Brodsky, F.M., et al. (2014). Actin scaffolding by clathrin heavy chain is required for skeletal muscle sarcomere organization. J. Cell Biol. *205*, 377–393.

Veiga, E., Guttman, J.A., Bonazzi, M., Boucrot, E., Toledo-Arana, A., Lin, A.E., Enninga, J., Pizarro-Cerdá, J., Finlay, B.B., Kirchhausen, T., et al. (2007). Invasive and Adherent Bacterial Pathogens Co-Opt Host Clathrin for Infection. Cell Host Microbe *2*, 340–351.

Wehrle-Haller, B. (2012). Assembly and disassembly of cell matrix adhesions. Curr. Opin. Cell Biol. *24*, 569–581.

Zuidema, A., Wang, W., Kreft, M., Te Molder, L., Hoekman, L., Bleijerveld, O.B., Nahidiazar, L., Janssen, H., and Sonnenberg, A. (2018). Mechanisms of integrin **α**V**β**5 clustering in flat clathrin lattices. J. Cell Sci. *131*.

Author contributions

LH designed research and performed most experiments.
AA performed experiments and performed all matlab image analysis.
A-SL designed and generated all knock-in cell lines.
MA performed the experiments for the detection of alternative splicing of clathrin.
JB and PK helped with the strategy for isolation of knock-in cell lines by flow cytometry.
HTM supervised the project during the initial observation.
LA-S designed research, conduct image analysis with imageJ scripts and supervised the project.
LH and LA-S wrote the manuscript with input from all authors.

Acknowledgments

We would like to thank the HILIFE light microscopy unit and the HiLIFE Flow Cytometry unit for technical assistance. We would like to thank Pekka Lappalainen, Markku Hakala and Tai Arima for the critical and kind reading of our manuscript. LA-S is supported by HiLIFE, the Academy of Finland (Research Fellow), Sigrid Juselius Foundation (Young PI grant), Finnish Diabetes Research Foundation, Magnus Ehrnrooth Foundation and Instruct-ERIC (R&D research award).

Materials and Methods

Cell culture and reagents

U2OS, U2OS-AP2-GFP and U2OS-AP2-GFP-ITGB5-mScarlet were cultured in MEM supplemented with 10 % fetal bovine serum (FBS) (Gibco) and penicillin-streptomycin (100 U/ml, Thermo Scientific).

The following primary antibodies were used: anti-human integrin beta 1 clones 12G10 (Novus bio, NB100-63255) and mAb13 (BD, 552828), anti-human integrin alpha v beta 5 clone 15F11 (Millipore MAB2019Z), anti-human p-paxillin Y118 (Cell Signaling, 69363) and anti-human p-FAK Y397 (Invitrogen, 44-624G). Corresponding secondary antibodies raised against rabbit or mouse IgG were from Jackson Immunoresearch.

Coating of imaging dishes

To compare the effect of several major extracellular matrix proteins on AP2 life-time, the glass coverslip areas (14 mm diameter) of imaging dishes (Mattek) were pre-coated with 1% (10 µg/ml, 300 µl in PBS) of the following ECM proteins: recombinant human fibronectin (Merck, 341631), recombinant human vitronectin (PeproTech, 140-09), collagen IV (Santa cruz, se-29010), and collagen I (Sigma, C3867) overnight at +37°C, or left untreated. Alternatively, as non-ECM protein controls, 1% BSA (Thermo Fisher, A34785) or poly-L-lysine (MP Biochemicals, 152690) were used. In further experiments FN coating was performed similarly.

To study local vs. global effects of FN, FN was mixed with 50 ng/ml of Alexa647-labelled BSA and used to precoat the imaging dishes overnight in +37°C. The coated surface was subsequently scratched with a needle to allow partial reappearance of glass. After scratching, the dishes were rinsed 3x with PBS. 20 000 U2OS-AP2-GFP cells were seeded on patterned imaging dishes to ensure sufficient single-cell attachment to border areas.

Overexpression of mammalian proteins.

The clathrin inhibitor AP180 c-terminal fragment (AP180ct; amino acids 516-898) cDNA, from rat origin was described previously (Ford et al., 2001). This construct was cloned into a Gateway compatible pCI vectors, containing an N-terminal monomeric EGFP using the Gateway system.

Transient transfections were carried out with PEI MAX transfection reagent (Polysciences, 24765-1) using 70% confluent U2OS cells.

Genetic engineering of cell lines

U2OS-AP2-GFP cell line

Three guide RNA (gRNA) sequences (Integrated DNA Technologies) were designed using the Welcome Sanger Institute Genome online editing tool (//https://wge.stemcell.sanger.ac.uk/). gRNAs were cloned into pSpCas9(BB)-2A-Puro (PX459) V2.0 (gift from. Feng Zhang, Addgene #62988) using BbsI sites and confirmed by sanger sequencing.

gRNAs were transfected with the donor template for homologous recombination and the most effective gRNA (TGCTACAGTCCCTGGAGTGA), judged by the percentage of fluorescent cells by FACS, was used for single clone selection, genotyping and confirmation by microscopy.

The donor template sequence was:

GGCCAGCATCCTGGGGGGCCTCGTCTCACCCCAGGGTCTCCCCTCACACAGGTTTACACGGTCGTGGACGAGATGTTCCTGGCTGGCGAAATCCGAGAGACCA
GCCAGACGAAGGTGCTGAAACAGCTGCTGATGCTACAGTCCCTGGAGGGAAGTGCATCTGGGAGCTCAGGCGCTAGTGGTTCAGCGAGCGGGGTGAGCAAG
GGCGAGGAGCTGTTCACCGGGGTGGTGCCCATCCTGGTCGAGCTGGACGGCGACGTAAACGGCCACAAGTTCAGCGTGTCCGGCGAGGGCGAGGGCGATG
CCACCTACGGCAAGCTGACCCTGAAGTTCATCTGCACCACCGGCAAGCTGCCCGTGCCCTGGCCCACCCTCGTGACCACCCTGACCTACGGCGTGCAGTGCTT

CAGCCGCTACCCCGACCACATGAAGCAGCACGACTTCTTCAAGTCCGCCATGCCCGAAGGCTACGTCCAGGAGCGCACCATCTTCTTCAAGGACGACGGCAAC
TACAAGACCCGCGCCGAGGTGAAGTTCGAGGGCGACACCCTGGTGAACCGCATCGAGCTGAAGGGCATCGACTTCAAGGAGGACGGCAACATCCTGGGGCA
CAAGCTGGAGTACAACTACAACAGCCACAACGTCTATATCATGGCCGACAAGCAGAAGAACGGCATCAAGGTGAACTTCAAGATCCGCCACAACATCGAGGAC
GGCAGCGTGCAGCTCGCCGACCACTACCAGCAGAACACCCCCATCGGCGACGGCCCCGTGCTGCTGCCCGACAACCACTACCTGAGCACCCAGTCCAAGCT
GAGCAAAGACCCCAACGAGAAGCGCGATCACATGGTCCTGCTGGAGTTCGTGACCGCCGCCGGGATCACTCTCGGCATGGACGAGCTGTACAAGTGAGGGC
AGGCGAGCCCCACCCCGGCCCCGGCCCCTCCTGGACTCGCCTGCTCGCTTCCCCTTCCCAGGCCCGTGGCCAACCCAGCAGTCCTTCCCTCAGCTGCCTAGGA
GGAAGGGACCCAGCTGGGTCTGGGCCACAAGGGAGGAGACTGC

where C terminal tagging with GFP is in green (codon-optimized) + short linker in purple. 150 bp homology arms (orange) were incorporated via PCR amplification from a synthesized (IDT), codon-optimized monomeric EGFP.
dsPCR product was purified and 150 ng was used directly for transfection together with gRNAs. 70-80% confluent 24 well of U2OS cells were transfected with 2 µl PEI (1 mg/ml), 150 ng of plasmid and 150 ng of the PCR product. Two days after transfection cells were treated with puromycin (1 µg/ml) to enrich for successfully transfected cells. After expansion, GFP-positive cells were sorted by FACS, and single clones were expanded and genotyped.

U2OS-AP2-GFP-ITGB5-mScarlet cell line

This cell line was produced by the same protocol as the U2OS-AP2-GFP cells with the following changes:

The gRNA sequence was CAAATCCTACAATGGCACTG, and the donor template was:

GGTTTGAGTGTGTGAGCTAACATGTGTCCTCATCCTCTTCCCCGCCGTGTTCTGTAGGCTTCAAATCCATTATACAGAAAGCCTATCTCCACGCACACTGTGGACTTCA
CCTTCAACAAGTTCAACAAATCATATAACGGCACTGTTGAC
GGAAGTGCATCTGGGAGCTCAGGCGCTAGTGGTTCAGCGAGCGGGgtgagcaagggcgaggcagtgatcaaggagttcatgcggttcaaggtgcacatggagggctccatgaa
cggccacgagttcgagatcgagggcgagggcgagggccgcccctacgagggcacccagaccgccaagctgaaggtgaccaagggtggcccccctgcccttctcctgggacatcctgtcccctcagt
tcatgtacggctccagggccttcatcaagcaccccgccgacatccccgactactataagcagtccttccccgagggcttcaagtgggagcgcgtgatgaacttcgaggacggcggcgccgtgaccgtg
acccaggacacctccctggaggacggcaccctgatctacaaggtgaagctccgcggcaccaacttccctcctgacggccccgtaatgcagaagaagacaatgggctgggaagcatccaccgagcg
gttgtaccccgaggacggcgtgctgaagggcgacattaagatggccctgcgcctgaaggacggcggccgctacctggcggacttcaagaccacctacaaggccaagaagcccgtgcagatgccc
ggcgcctacaacgtcgaccgcaagttggacatcacctcccacaacgaggactacaccgtggtggaacagtacgaacgctccgagggccgccactccaccgg
cggcatggacgagctgtacaagTAA
TGTTTCCTTCTCCGAGGGGCTGGAGCGGGGATCTGATGAAAAGGTCAGACTGAAACGCCTTGCACGGCTGCTCGGCTTGATCACAGCTCCCTAGGTAGGCACCA
CAGAGAAGACCTTCTAGTGAGCCTGGGCCAGGAGCCCACAGTGCCT

where A = silent mutations in 5′ HA, linker region is in purple, and mScarlet is in orange.

Lentiviral shRNA production and transduction

Lentiviruses for shRNA production were made using packaging plasmids pCMVR and pMD2.g and specific shRNAs in pLKO.1 vector as follows: 80% confluent HEK293T cells in DMEM supplemented with 10% FBS and 100U penicillin-streptomycin were transfected using PEI MAX transfection reagent. 5 hours later, the medium was changed to DMEM supplemented with 4% FBS and 25mM HEPES. Media containing lentiviral particles were harvested after 48 and 72 hours, filtered (0.45 µm), aliquoted and stored in -80°C.

U2OS-AP2-GFP were transduced with lentiviral media expressing respective shRNAs in the presence of Polybren 8 µg/ml (Sigma-Aldrich, TR-1003) for 5 hours, and replaced with culture medium. 48 h later, puromycin (1 µg/ml) was added for 24 h to allow selection of transduced cells. Experiments targeting AP2 subunits were performed otherwise similarly but without puromycin selection. All shRNA silenced cell lines were replated to glass-bottomeed imaging dishes one day prior to imaging.

The following sequences were targeted:

Integrin beta 5 targeting (ITGB5) shRNAs: TRCN0000057744 (GCATCCAACCAGATGGACTAT), TRCN0000057745 (GCTGTGCTATGTTTCTACAAA)

Integrin beta 1 targeting (ITGB1) shRNAs: TRCN0000029644 (CCTGTTTACAAGGAGCTGAAA), TRCN0000029645 (GCCTTGCATTACTGCTGATAT)

AP2 sigma 1 targeting (AP2S1) shRNAs: TRCN0000060263 (GACGCCAAACACACCAACTTT), TRCN0000060266 (GTGGAGGTCTTAAACGAATAT), TRCN0000060267 (CACAACTTCGTGGAGGTCTTA).

AP2 alpha 1 (AP2A1) targeting shRNAs: TRCN0000065108 (GCTGAATAAGTTTGTGTGTAA), TRCN0000065109 (GCACATTGACACCGTCATCAA)

Clathrin exon 31 analysis

Cell culture dishes were coated with 10 µg/ml of FN in a cell culture incubator, or left uncoated. Next day, U2OS cells were plated to reach confluency in 24 h. RNA extraction, cDNA synthesis, and PCR followed those described by Moulay et al. (2020) with minor variations. Total RNA was extracted from cells using TRIzol reagent with an additional acidic phenol (pH 5.4) extraction step to remove genomic DNA contamination. cDNA synthesis from 1 µg total RNA was carried out RNA using Maxima H Minus Reverse Transcriptase (Thermo Fisher Scientific) and oligo dT12–18 (Life Technologies). No enzyme reactions were included to confirm that no genomic DNA was present. PCR was performed using Phusion High-Fidelity DNA polymerase (Thermo Fisher Scientific) with no other variations from Moulay et al., (2020). Primers used were: F' TGC CCT ATT TCA TCC AGG TCA, R' ATG GGT TGT GTC TCT GTA GC. Gel images were acquired using a GelDoc XL (Bio Rad).

Microscopy

All live videos and images from fixed samples were acquired with an ONI nanoimager microscope equipped with 405, 488, 561 and 647 lasers, an Olympus 1.4NA 100x super achromatic objective and a Hamamatsu sCMOS Orca flash 4 V3 camera.

Endogenous AP2 life-time monitoring

35 000 U2OS-AP2-GFP cells were plated to precoated/glass area of the dish resulting in approximately 70-80% confluency 20 h later, at the onset of imaging. Alternatively, shRNA silenced cell lines were plated. After overnight culture, 25 µM HEPES was added and samples were subjected to live TIRF imaging in a pre-heated +37°C chamber.

The ONI nanoimager microscope set to TIRF angle was used to acquire AP2 lifetimes at the cell membrane from 300 frames (1 frame/s) with the exposure time of 330 ms. Each video represents endocytic events from 2-3 cells.

Acute manipulation of integrin activity

Acute modulation of ligand binding activity for integrin **β**1 was achieved using the function blocking antibody mab13 (0.3 µg/ml). U2OS-AP2-GFP cells were plated on FN as explained above, mab13 was added, and 5 min time lapses were continuously collected 5 min after the addition of mab13 until 35 min, control videos (time point 0) had no mab13 added.

To acutely induce the formation of FCL and RAs we used the small molecular inhibitor Cilengitide (MedChem Express HY-16141, 10uM). U2OS-AP2-GFP-ITGB5-mScarlet cells plated on uncoated imaging dishes were treated with Cilengitide for 15 min, washed twice, and imaged with the ONI nanoimager microscope at TIRF angle at 30 s intervals, with an exposure time of 100 ms for AP2 and 300 ms for integrin-**β**5.

Immunofluorescent staining and imaging

For immunofluorescent studies, cell were fixed with 4% paraformaldehyde-PBS for 15 min in a +37°C incubator, washed with PBS and blocked with 1% BSA-PBS. Primary antibodies diluted in 1% BSA-PBS were incubated for 1 h, samples were washed with PBS, and secondary antibodies diluted in 1% BSA-PBS were let to bind for 30 min. Samples were imaged with the ONI nanoimager microscope using TIRF angle and exposure times of 500 ms or 1000 ms.

Manipulation of CME machinery to study RA formation

Clathrin assembly at the cell membrane was reduced by silencing two subdomains of AP2, or by overexpressing AP180ct, which acts as a dominant negative for AP2. U2OS AP2-GFP cells silenced for AP2A1 shRNA #1 and #2 or AP2S1 shRNA #1, #2 and #3, and control shRNA, and plated on uncoated imaging dishes were fixed and stained for integrin **α**v**β**5 and FA marker p-PAX. Alternatively, AP180ct was overexpressed in U2OS AP2-GFP cells and cells were plated on uncoated imaging dishes, fixed the next day, and stained for integrin **α**v**β**5 and p-PAX. RA formation (integrin **α**v**β**5 adhesions w/o FA marker) and FAs (integrin **α**v**β**5 colocalising with FA marker) were imaged using TIRF microscopy.

Manipulation of integrin activity and availability

We performed time series experiments to block integrin **β**1 active conformation with the mab13 antibody or to inhibit integrin **α**v**β**5 with Cilengitide. Experiments utilizing mab13 were performed with U2OS-AP2-GFP cells plated on FN coated dishes to disfavour the preformation of FCLs and RAs. Mab13 (0.3 µg/ml) was added to replicate samples and fixed 15, 30 or 45 min later. Similarly, U2OS-AP2-GFP cells plated on uncoated dishes to favour the preformation of FCLs and RAs, were treated with Cilengitide. Samples were stained for integrin **α**v**β**5 and FA marker p-PAX.

Alternatively, after 15 min of Cilengitide treatment, samples were washed and fixed at several time points (Fig. S8) after Cilengitide washout to monitor reappearance of FCL and RAs.

U2Os-AP2-GFP cells silenced for integrin **β**1 or **β** 5 and control were plated either on FN coated dishes (control shRNA and ITGB1 shRNAs) or on uncoated (glass) dishes (control shRNA and ITGB5 shRNAs), and fixed the next day. Samples were stained for integrin **α**v**β**5 and FA marker p-PAX and imaged using TIRF microscopy.

Image analyses

CME lifetime analyses (FCL frequency)

To track CME events and measure lifetimes we used 'u-track 2.0' multiple-particle tracking MATLAB software at default settings (Jaqaman et al., 2008). To determine the frequency of FCLs, we counted the number of pits (events lasting longer than 20 s and shorter than 120 s) and the number of FCLs (events lasting longer than 120 seconds, as described in (Saffarian et al., 2009)) in every frame, and calculated the FCL frequency (number of FCLs/number of FCLs + number of pits). Mean FCL frequency was taken as the average FCL frequency of all frames more than 120 seconds from the beginning and the end of each video.

Qualitative analysis of RAs

U2OS-AP2-GFP-ITGB1-mScarlet cells fixed at several time points after Cilengitide washout were analysed for reappearance of RAs (Fig. S8). The samples were sub grouped into four categories (0-3), according to the stage of RA-development. Group 0 (green) had no RAs, group 1 (orange) had few dot-like RAs (punctate integrin **α**v**β**5+FCL, no p-PAX), group 2 (purple) had many dot-like RAs and a few bigger RAs, and group 3 (blue) had several big RAs.

Other analyses:

With the exception of FCL frequencies, all image analyses were performed using imageJ. Simple fluorescence measurements were done using manually. Others were performed using custom scripts as shown below:

RA coverage (Figs 3b, 3d, 5d)

Individual cells were marked and ITGB5 and P-PAX channels were segmented using the Robust Automatic Threshold Selection function. RAs were defined as ITGB5 signals not colocalizing with p-PAX. The area of RAs were then dived by the area of each marked cell to obtain RA coverage.

AP2-ITGB5 dynamics (Fig. 3g)

Events showing the appearance of both AP2 and ITGB5 were identified by visual inspection of videos. For the generation of graphs, we selected only events where we could unambiguously ensure that significant FCLs and ITGB5 signals were not present in the region for at least 3 minutes. Time zero was defined as the frame where AP2 signal appeared and fluorescence Intensity from a 10μm x 10μm region around each event was measure for 3 minutes before (6 frames) and 5 minutes after (10 frames). Fluorescence was normalised to the highest value in these frames.

AP2 intensity per colocalisation status (Figs 4b, S5b, S2b)

AP2, ITGB5 and P-PAX channels were segmented using the Robust Automatic Threshold Selection function. Each segmented AP2 spot had the fluorescence intensity measured from the original image and classified for its colocalisation with either markers (ITGB5 or p-PAX). We used full images for these analyses.

RAs colocalising to AP2 (Fig. 4c)

Individual cells were marked and AP2, ITGB5 and P-PAX channels were segmented using the Robust Automatic Threshold Selection function. RAs were defined as ITGB5 signals not colocalizing with p-PAX. In the conditions used of these experiments, (FN + mab13) RAs we primarily individual spots. The colocalisation of RAs to AP2 was classified by measuring the intensity of each RA region at the segmented AP2 channel.

FN intensity vs AP2 intensity (Fig. S1b)

AP2, ITGB5 and P-PAX channels were segmented using the Robust Automatic Threshold Selection function. Each segmented AP2 spot had the fluorescence intensity measured from the original image. A 3μm x 3μm region was drawn around each AP2 spot and used to measure the intensity of FN from the original image. Data is presented as the fluorescence for each AP2 spot.

Statistics

All results were repeated at least 3-5 times. Figure legends state the exact n-values used in analyses. For multiple comparisons one-way ANOVA was performed followed by Tukey's multiple comparison. Pairwise comparisons were performed using two-tailed Student's t-test with equal variance. All graphs and statistical calculations were performed in GraphPad